Structure and stability of multiple micro-droplets

Jan Guzowski, Piotr M. Korczyk, Piotr Garstecki

Supporting Information

In the following we use square brackets to refer to equations from the main text of the paper.

I. STABILITY DIAGRAM FOR DOUBLE DROPS.

In Fig. 1 we plot contour lines on the stability diagram corresponding to the condition $\cos\theta_j = const = c$ for various values of the constant c in the case of a double droplet (eq. [3]). One can clearly distinguish the limiting cases mentioned in the main text:

(i) $\gamma_i \to \gamma_{ij}$ and $\gamma_j/\gamma_{ij} \to 0$. In terms of c eq. [5] can be rewritten as

$$\gamma_j/\gamma_{ij} = \frac{1}{c}(\gamma_i/\gamma_{ij} - 1). \tag{1}$$

In this limit different c correspond to straight lines on the stability diagram with different slopes but all converging to a single point $(\gamma_i/\gamma_{ij} = 1, \gamma_j/\gamma_{ij} = 0)$. For $j = A, B$ see Figs. 1a, 1b, respectively.

(ii) $\gamma_{ij} \to \gamma_i$ and $(\gamma_i - \gamma_j)/\gamma_{ij} \to 0$. Eq. [6] can be rewritten in terms of c as

$$\gamma_j/\gamma_{ij} = \gamma_i/\gamma_{ij} - c. \tag{2}$$

Accordingly, in this limit different c correspond to straight parallel lines with the same slope equal to 1 but with different vertical shifts c.

Outside the limiting linear regions there is a transition region (approximately for $\gamma_i/\gamma_{ij} \in [0.2, 4]$) in which the lines $\cos\theta_j = const$ are not straight.

II. CALCULATION OF THE CURVATURE OF THE INTERNAL INTERFACE OF PERFECT JANUS DROPS.

In the case of three-dimensional double Janus drops the line $k^*(\theta_B)$ separating the regions of positive and negative curvatures R^{-1} in the (θ_B, k) plane (solid line in Fig. 2*a*) is given

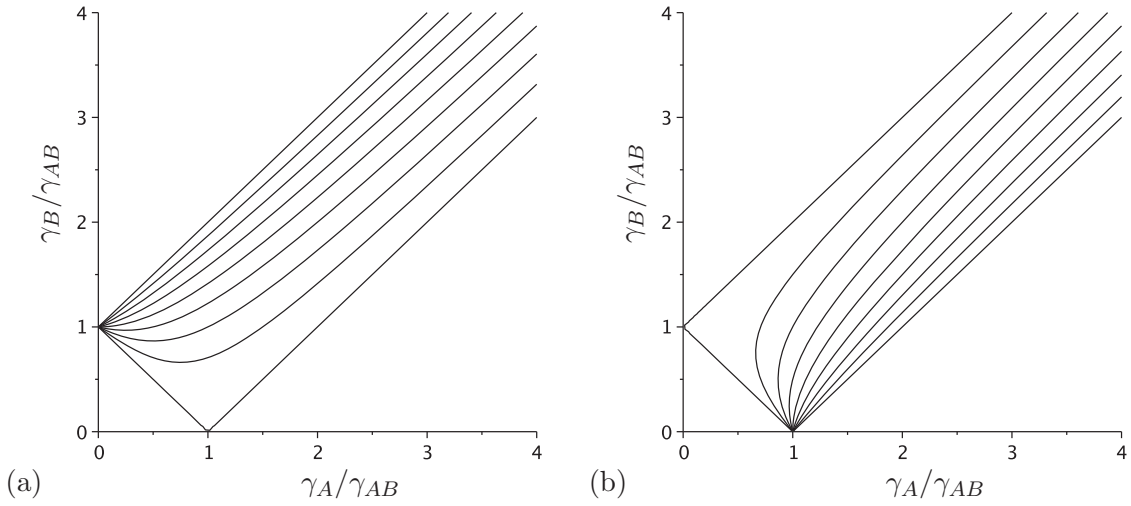

Figure 1: (a) Lines of constant $\cos\theta_A = c$ (eq. [3]) for $c = 1, 0.75, 0.5, 0.25, 0, -0.25, -0.5, -0.75, -1$ (from top to bottom). (b) Lines of constant $\cos\theta_B = c$ (the same values as in (a) but from bottom to top). Note that in both cases in the limit of large γ_A and γ_B the lines are parallel and have equal spacing due to the constant increment $\Delta c = 0.25$ between the neighboring lines.

by the following equation (analogical to eq. [10]):

$$k^*(\theta_B) = \frac{f_0(\theta_B)}{1 - f_0(\theta_B)}. \tag{3}$$

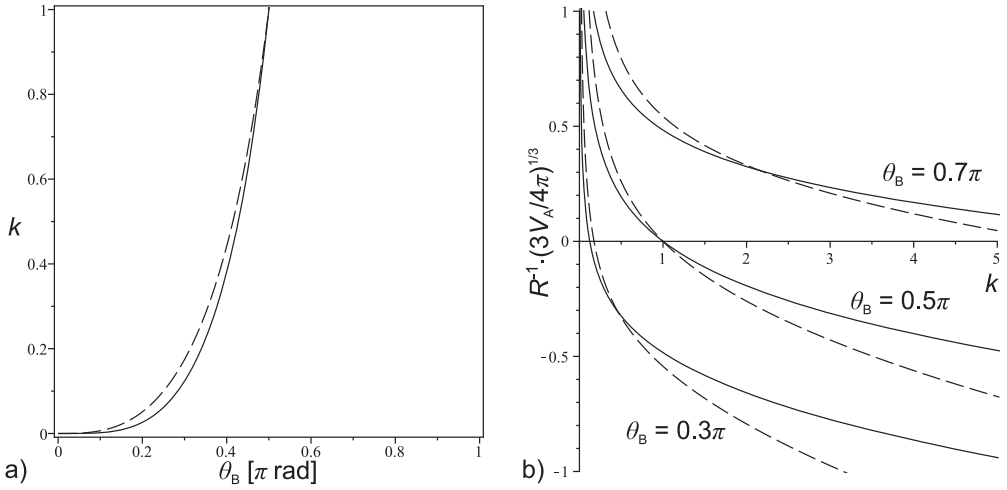

Figure 2: (a) Lines of zero curvature $R^{-1}(\theta_B, k) = 0$ (eqs. (3) and [10]) in the case of three- and two-dimensional drops (solid and dashed lines, respectively). (b) Parametric plot of $R^{-1}(\theta_B, k)$ (eqs. (4) [11] and [9]) for fixed three different values of θ_B (the style of lines the same as in (a)).

In analogy to eq. [11] we also have

$$k = k(\theta_B, \beta) = \frac{R_B^3 f_0(\theta_B) + R^3 f_0(\theta_B - \beta)}{R_B^3 f_0(\theta_B) - R^3 f_0(\theta_B - \beta)}. \tag{4}$$

Solving eqs. (4) and [9] with respect to R we obtain $R^{-1} = R^{-1}(\theta_B, k)$, which is plotted for several values of θ_B in Fig. 2*b*.

III. SPHERICAL CAP.

For the graphical definition of a spherical cap with an opening angle θ, see Figure 3.

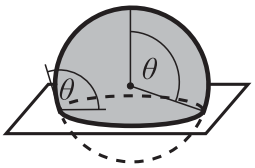

Figure 3: A plane intersecting a spherical drop divides it into two spherical caps - one (marked in grey) with an opening angle θ and the other with an opening angle $\pi - \theta$.

IV. CALCULATION OF THE STABILITY DIAGRAMS FOR MULTIPLE JANUS DROPS.

In the following we determine the shape of the liquid lenses forming a multiple Janus drop, given the ratio of volumes $k = V_B/V_A$ and the contact angles θ_A and θ_B under the assumption that all the segments of the same phase are identical, i.e., that they form a periodic chain (section of the shortest repeating unit is sketched in Figure 4).

First we determine the auxiliary angles β_A and β_B as functions of the radii R_A and R_B and the contact angles. The following relation holds:

$$\beta_A + \beta_B + \theta_A + \theta_B = 2\pi. \tag{5}$$

Additionally, from the law of sines for the triangle O_1O_2P (Fig. 4) we have

$$R_A \sin\beta_A = R_B \sin\beta_B, \tag{6}$$

which together with eq. (5) after applying basic trigonometric identities yields

$$\tan\beta_i = -\frac{R_j \sin(\theta_A + \theta_B)}{R_i + R_j \cos(\theta_A + \theta_B)}, \tag{7}$$

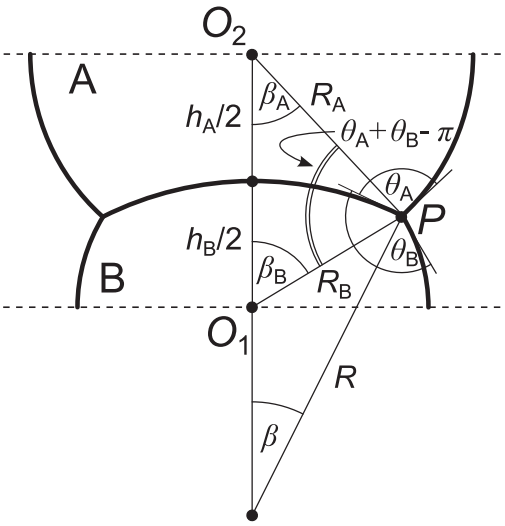

Figure 4: Sketch of the section of the repeating unit of the multiple drop with graphical definition of the basic parameters.

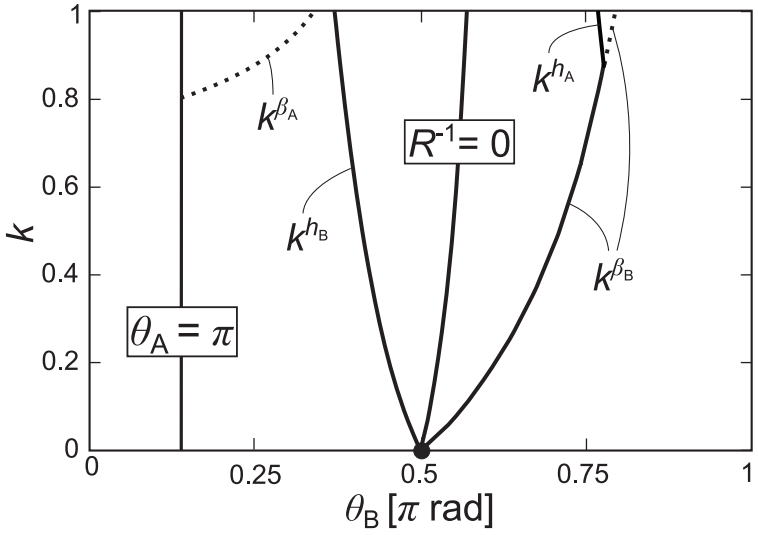

Figure 5: The morphologic transition lines of a multiple drop for $\bar{\theta} = 1.15\pi$ calculated numerically using Maple (solid lines) and Surface Evolver (dotted lines).

with $i = A, B$. The auxiliary angle β fulfills (see Figure 4)

$$\beta = \theta_B + \beta_B - \pi. \tag{8}$$

The heights h_i of the segments can be expressed as

$$h_A/2 = R_A \cos\beta_A - R\big(1 - \cos\beta\big), \tag{9}$$

$$h_B/2 = R_B \cos\beta_B + R\big(1 - \cos\beta\big), \tag{10}$$

where R can be either positive or negative. The condition of the balance of Laplace pressures yields the same result as for double Janus drops, i.e., (repeating eq. [8])

$$R = \left(\frac{\sin\theta_B}{R_A} - \frac{\sin\theta_A}{R_B} \right)^{-1} \sin(\theta_A + \theta_B). \tag{11}$$

Now β_i, β and R are all functions of $\theta_A, \theta_B, R_A, R_B$. In order to change the independent variables from the unknown radii R_i to the given volumes V_i one has to solve numerically the set of equations

$$3V_A/(4\pi) = R_A^3(1 - 2f_0(\beta_A)) - 2R^3 f_0(\beta), \tag{12}$$

$$3V_B/(4\pi) = R_B^3(1 - 2f_0(\beta_B)) + 2R^3 f_0(\beta) \tag{13}$$

with respect to R_A and R_B, where $f_0(\theta) = (2 + \cos\theta)\sin^2(\theta/2)$. By choosing the length scale such that $V_A = 1$ and $V_B = k$ one thus obtains $h_i = h_i(\theta_A, \theta_B, k)$, $\beta_i = \beta_i(\theta_A, \theta_B, k)$ and $R = R(\theta_A, \theta_B, k)$. The conditions $h_i = 0$ and $\beta_i = \pi/2$ correspond to the limits of stability beyond which the segments must either deform or coalesce. For example, for a fixed value of $\bar\theta =: \theta_A + \theta_B$ the transition lines can be calculated in the (θ_B, k) plane by solving numerically the set of equations $h_i(\bar\theta - \theta_B, \theta_B, k) = 0$ and $\beta_i(\bar\theta - \theta_B, \theta_B, k) = \pi/2$ for $i = A, B$. This yields four transition lines: $k = k^{(h_A)}(\theta_B)$, $k = k^{(h_B)}(\theta_B)$, $k = k^{(\beta_A)}(\theta_B)$ and $k = k^{(\beta_B)}(\theta_B)$. Depending on the value of $\bar\theta \in [\pi, 2\pi]$ the lines $k^{(h_i)}$ and $k^{(\beta_j)}$, $i \neq j$, can either (i) intersect with each other (for $\bar\theta \in [\pi, \bar\theta^*]$, where $\bar\theta^*$ is a certain angle which can be calculated numerically; we estimate $\bar\theta^* \simeq 1.25\pi$, see Fig. 4b in the main text) or (ii) intersect with the line $\theta_j = \pi$ (for $\bar\theta \in [\bar\theta^*, 2\pi]$). In the first case (i) the continuation of the lines $k^{(\beta_i)}$ beyond the intersection points corresponds to the transition from the metastable to the unstable region. However, this continuation cannot be calculated within our model with spherical interfaces. The deformed shapes of the segments in this case can be calculated numerically by finite-element minimization of the interfacial energy using, e.g., the software Surface Evolver (see the dotted line in Fig. 5).

We note that in Fig. 5 the lines $k^{(h_B)}$ and $k^{(\beta_B)}$ meet at the single point $(\theta_B = \pi/2, k = 0)$. This property can be actually proved for arbitrary $\bar\theta$. Assume that we approach the line $k^{(\beta_B)}$ from the 'stable' side, i.e., $\beta_B \nearrow \pi/2$ and simultaneously we take the limit $k = V_B \to 0$ (we set $V_A = 1$). Then from eq. (13) in which the left hand side vanishes and from the fact that $f_0(\beta_B \nearrow \pi/2) \nearrow 1/2$ we have $R^3 f_0(\beta) \to 0$, which together with $f_0(\beta) \sim \beta^4$ implies $\beta \to 0$. Next, we use another geometric relation: $\sin\beta = |R|^{-1} R_B \sin\beta_B$ (see Fig. 4), from which it

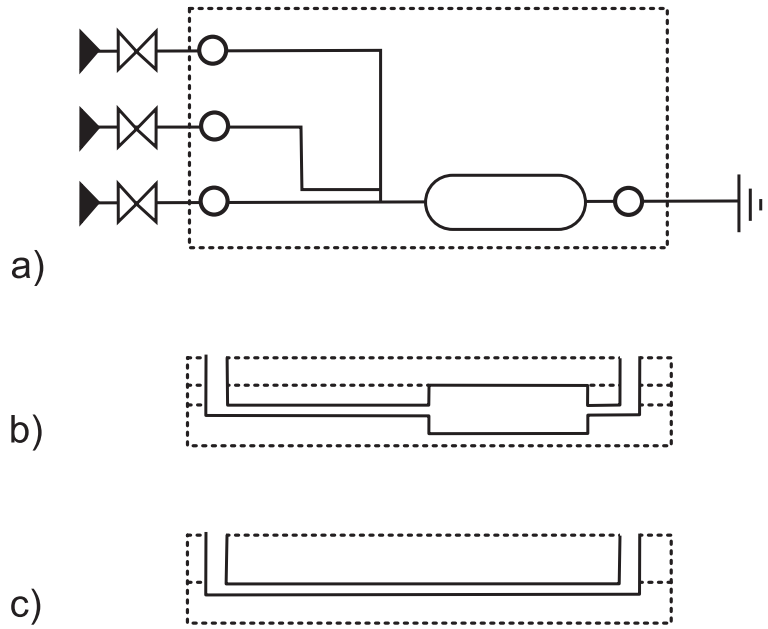

Figure 6: (a) Top-view of a schematic representation of the microfluidic device with two nested T-junctions used for generation of double and multiple drops. Pressure sources (►), valves (⋈) and inlets/outlets (○) to the chip (with the chip marked by dotted line) are indicated. (b) Side-view of the chip made of three layers of polycarbonate. The use of the middle layer enables positioning of the inlet to the chamber at the mid-height of the chamber. (c) Side-view of the chip made of two layers two layers of polycarbonate. In this case the chamber has the same depth as the channels.

follows that $\beta \sim |R|^{-1} R_B$, which implies $|R|^{-1} R_B \to 0$. Now, we need to check if in this limit R_B remains finite. From eqs. (5) and (6) we obtain $R_B = R_A \sin(\bar{\theta}_1)$, where $\bar{\theta}_1 = 3\pi/2 - \bar{\theta}$. Next from eq. (12) with $V_A = 1$ we finally get $R_B^3 = 3\sin^3(\bar{\theta}_1)/[4\pi(1 - 2f_0(\bar{\theta}_1))]$, i.e., R_B remains finite. This implies $|R|^{-1} \to 0$. Similarly, eq. (10) reduces to $h_B = R\beta^2 \sim |R|^{-1} R_B^2$ which implies $h_B \to 0$. This altogether shows that the lines $k^{(\beta_B)}$, $k^{(h_B)}$ and the line $R^{-1} = 0$ approach each other in the limit $k \to 0$. Finally, from eq. (8) it follows that in this limit we also have $\theta_B \to \pi/2$. Analogous reasoning applies to the case $k \to \infty$.

V. MICROFLUIDIC DEVICES

Schemes of the microfluidic devices are shown in Fig. 6.